Ab initio theory of defect scattering in spherical whispering-gallery-mode resonators

J. T. Rubin and L. Deych

Department of Physics, Queens College of the City University of New York (CUNY), Flushing, New York 11367, USA

(Received 10 September 2009; revised manuscript received 18 February 2010; published 18 May 2010)

An exact formalism for the interaction of a spherical whispering-gallery-mode (WGM) microresonator with an externally or internally placed subwavelength scatterer is developed. The experimentally observed doublets in the spectra of high-Q microspheres are shown to correspond to the ideal Mie resonance and a defect-induced resonance, while for TM-polarized WGMs a third peak is predicted. Explicit expressions for positions and widths of these new resonances are derived.

DOI: 10.1103/PhysRevA.81.053827 PACS number(s): 42.25.Bs

I. INTRODUCTION

Elastic (with no change in frequency) scattering of light due to particles with subwavelength dimensions is one of the most fundamental and intensively studied optical phenomena. Since Lord Rayleigh's [1] famous papers explaining why the sky is blue, it has been customary to refer to this phenomenon as Rayleigh scattering. While usually this term is used to describe the interaction between free propagating electromagnetic waves and small scatterers, recent technological developments have focused attention on the interaction between spatially confined optical fields and subwavelength particles. This situation arises, for instance, when whispering gallery modes (WGMs) of optical microresonators [2] interact with the resonators' morphological imperfections. Since the scatterers in this case are usually much smaller than the wavelength of light, this phenomenon is referred to as Rayleigh scattering of WGMs [3]. Given the fundamental nature of this process and its importance in applications of microresonators it is not surprising that it has attracted a significant amount of attention in recent years [3–7]. However, while scattering of free propagating light is a mature field for which many approaches have been developed [8], the study of scattering of WGMs is still in its infancy. Current understanding of this process relies on simple phenomenological models [3,7,9], but no fundamental theoretical description of this phenomenon has been developed so far.

While WGMs can occur in various types of geometries [10], we focus here on spherical microresonators. WGMs in this case correspond to Mie resonances [11] with ultranarrow widths, $\gamma_{l,s} \ll \omega_{l,s}$, where $\omega_{l,s}$ is the frequency of the mode, and respectively high (up to 10^9 for silica microspheres [10]) Q factors defined as $Q_{l,s} = \omega_{l,s}/\gamma_{l,s}$. WGMs are characterized by polar and azimuthal indexes, l and m, and a radial number s specifying, respectively, the angular and radial dependence of the fields in a spherical coordinate system centered at the sphere. The resonance frequency $\omega_{l,s}$ does not depend on the azimuthal number, which reflects the degeneracy of the resonances due to full spherical symmetry of the system. WGMs are also characterized by their mode volume, which can be very different for modes with the same l but different m. Modes with the smallest volume correspond to $|m| = l$, and $s = 1$ in which case the field is concentrated mostly in the equatorial plane and at the surface of the sphere. Such modes are called fundamental and their interaction with defects is of the primary interest.

It has been known for some time that the experimental spectra of WGMs are more complex than expected from standard Mie theory for ideal spheres. In particular, in place of an expected single ultranarrow resonance, one often observes an apparent asymmetric doublet with a diminished Q factor. This effect is common to the spectra of most microresonators and has been attributed to Rayleigh scattering of WGMs due to morphological inhomogeneities introduced during fabrication. The existing explanation of this effect is based on the backscattering hypothesis [4], which assumes that Rayleigh scattering couples fundamental WGMs of orbital number L with opposite signs of the azimuthal number $m = \pm L$ (counterpropogating modes). This coupling breaks the $\pm m$ degeneracy and gives rise to the spectral doublet. The degraded Q factor is prescribed to defect-induced coupling between WGMs and radiative modes and is accounted for by adding a scattering loss to the total losses of the resonator. In Ref. [7] these losses have been calculated for microdisk resonators using a semiphenomenlogical surface current method. The benefit of this approach is the simplicity of its associated physical picture and its apparent ability to explain qualitatively some of experimentally observed effects.

However, the apparent agreement with an experiment cannot replace a rigorous theoretical description based on fundamental principles (Maxwell equations in this case) rather than on phenomenological *ad hoc* assumptions. Moreover, we show here that in the particular case of microspheres the backscattering paradigm seriously oversimplifies the problem and as a result misses a number of important features of the phenomenon under discussion. More specifically, the backscattering approach ignores the fact that the loss of symmetry resulting from scatterers breaks the degeneracy of and therefore couples all azimuthal components, $-L \leqslant m \leqslant L$ and not just counterpropagating modes. At the very basic level this approach treats an essentially quasi-two-dimensional problem in a one-dimensional approximation. The backscattering paradigm, at least in its current implementations, also ignores the vector nature of light, which in the situation under consideration, manifests itself as a dependence of the strength of interaction between WGM and scatterer upon the orientation of the dipole moment of the latter and on the polarization of the excited WGM.

Recently, the controlled scattering experiments of Ref. [9] showed that a single external dipole scatterer positioned close to the surface of the sphere resulted in effects which are

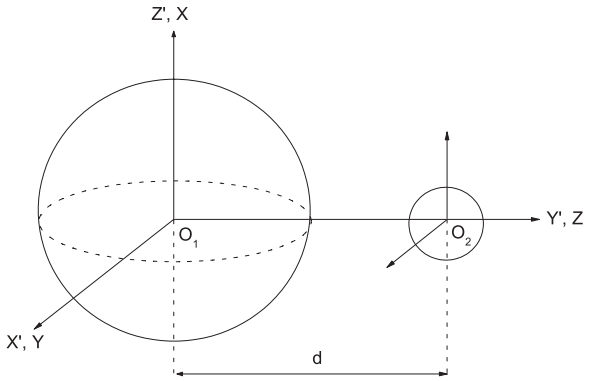

FIG. 1. Coordinate systems used in calculations.

qualitatively similar to those attributed to surface roughness. Theoretically, this is a consequence of the fact that under weak scattering, random inhomogeneities in the structure of the resonator interact with light like independent dipole scatterers. The results of Ref. [9] demonstrate the importance of understanding the interaction between WGMs in microspheres and a single subwavelength defect. The main objective of this article is to develop an *ab initio* theory of this phenomenon. The theory developed herein not only provides a conceptual framework for understanding the experiments of Ref. [9] on the basis of fundamental principles, but also constitutes a significant first step toward a general microscopic theory of scattering of WGMs. In this theory, which is based on direct solution of Maxwell equations and does not use any *ad hoc* assumptions, spectral splitting and broadening of resonances arise in a natural way. In addition, it predicts and describes such less-explored effects as scattering-induced polarization conversion, which was recently observed experimentally [12]. For completeness, we consider defects positioned both outside and inside the microresonator. Such an internal defect could, for example, be a small local fluctuation in the dielectric permittivity formed during the fabrication process or can be introduced intentionally.

The main assumption of the theory is that, since defects are small enough to be treated as dipole scatterers, their precise shape is irrelevant and can be taken to be spherical. In this way the problem is reduced to describing two electromagnetically coupled spheres of radii R_1 and $R_2 \ll R_1$ with refractive indexes n_1 and n_2, respectively, whose centers are positioned at a distance d from each other (see Fig. 1). The whole system is assumed to be situated in an external medium of refractive index n_0. The problem of two (or more) spheres coupled by the evanescent field of their WGMs has been previously discussed in several papers [13–15], where MSMT based on modal expansion of the electromagnetic field was used. In this article we advance previous studies by showing that when one of the interacting spheres can be treated as a dipole, the equations for modal expansion coefficients can be solved exactly so that they can be obtained in a closed form.

II. MIE THEORY FOR INTERNALLY AND EXTERNALLY COUPLED TWO-SPHERE SYSTEMS

Our goal in this article is to find the resonance frequencies and the complete field distribution of the two-sphere system subject to an external excitation. The general framework for electromagnetic scattering by an aggregate of spheres is known as multisphere Mie theory (MSMT) and gives, in principle, exact results. An extensive literature exists on MSMT, beginning with the authoritative work of Bruning and Lo on scattering by two spheres [16,17], see also an article by Fuller [13]. The generalization to more than two spheres can be found in Refs. [18,19], with a more detailed analytical approach in Ref. [20]. The structure and resonance frequencies of high-order WGMs in two identical spheres are discussed in Refs. [14,15]. The case where one sphere resides completely within another is discussed in several works [21–23], with results focusing mainly on general scattering properties with plane-wave illumination. Partial results from this article have been published previously in Ref. [24].

The current work focuses on electromagnetic properties of a particular two-sphere system, where one of the spheres is large enough to support high-order WGMs, while the second sphere is of a subwavelength dimension and behaves essentially as a dipole. Since the incident wave is assumed to excite a single WGM in the larger sphere, the situation can be described as scattering of the excited WGM due to the subwavelength defect. Depending on the mutual position of the defect and the main sphere (the resonator), two cases must be distinguished. The defect can reside outside the resonator, in which case it couples to the resonator's scattered field (external coupling). One can also envision a situation where the defect is completely inside the resonator and couples to its internal field (internal coupling). The standard MSMT framework is based on the external coupling configuration and can therefore be directly applied to the former case. The internal coupling situation, on the other hand, is inconsistent with the field expansions used in Refs. [13–20]. The inconsistency manifests itself as a divergence of the multipole expansion for the field when the two spheres are separated by a distance $d < (R_1 + R_2)$. Therefore, the modified MSMT utilized in Refs. [21–23] is employed. However, because this configuration is much less well known and is usually treated in the literature under the assumption of plane-wave illumination, we rederive the modified MSMT framework for the case of an arbitrary incident field before applying it to the situation considered here.

Treatment of both the internal and the external coupling scenarios is based on expansion of all relevant fields in terms of vector spherical harmonics (VSH) defined in coordinate systems with origins at the center of each sphere. Figure 1 shows the configuration under consideration together with coordinate systems relevant to the problem. The coordinate systems centered at the larger sphere and the defect (points O_1 and O_2, respectively) are shifted with respect to each other by distance d along a common axis. The Maxwell equations are first solved for each sphere separately, giving scattered, $\mathbf{E}_{\mathrm{sc}}$, and internal, $\mathbf{E}_{\mathrm{int}}$, fields as linear combinations of VSH with as yet undetermined coefficients:

$$\mathbf{E}^{(i)}_{\mathrm{sc}}(\mathbf{r}_i) = E_0 \sum_{l,m} \left[a^{(i)}_{l,m} \mathbf{N}^{(3)}_{l,m}(\mathbf{r}_i) + b^{(i)}_{l,m} \mathbf{M}^{(3)}_{l,m}(\mathbf{r}_i) \right], \quad (1)$$

$$\mathbf{E}^{(i)}_{\mathrm{int}}(\mathbf{r}_i) = E_0 \sum_{l,m} \left[c^{(i)}_{l,m} \mathbf{N}^{(1)}_{l,m}(\mathbf{r}_i) + d^{(i)}_{l,m} \mathbf{M}^{(1)}_{l,m}(\mathbf{r}_i) \right]. \quad (2)$$

We also assume that an incident field $\mathbf{E}_{\rm inc}$ can be expressed in terms of VSH by the expansion

$$\mathbf{E}^{(i)}_{\rm inc}(\mathbf{r}_i) = E_0 \sum_{l,m} \left[\eta^{(i)}_{l,m}\mathbf{N}^{(1)}_{l,m}(\mathbf{r}_i) + \zeta^{(i)}_{l,m}\mathbf{M}^{(1)}_{l,m}(\mathbf{r}_i)\right]. \quad (3)$$

Here index i numerates the spheres $i = 1,2$ with $i = 1$ corresponding to the larger sphere and each position vector $\mathbf{r}_i$ is defined in the local coordinate system. Functions $\mathbf{N}^{(j)}_{l,m}$ and $\mathbf{M}^{(j)}_{l,m}$ are the VSH fields of TM and TE polarization, respectively [8], with $j = 1$ or $j = 3$ indicating radial dependencies given by either the spherical Bessel function $[j_l(x)]$ or the Hankel function $[h^{(1)}_l(x)]$ of the first kind, respectively. They take dimensionless frequency $x = kr$, with wave vector $k = nk_0 = n\omega/c$, where n is the refractive index of the region in which the respective field is defined. The corresponding magnetic fields, $\mathbf{H}$, are determined from the same coefficients by switching $\mathbf{N}_{l,m}$ and $\mathbf{M}_{l,m}$ and multiplying by $-i\sqrt{\epsilon/\mu_0}$ [16], where ϵ and μ_0 are, respectively, the dielectric permitivity and permeability of the region (we consider only nonmagnetic media).

Presentation of the incident field in the form of Eq. (3) is standard for the theory of Mie scattering, as one usually considers the incident wave to be a plane wave. However, in the situation considered here the incident wave is typically a mode of a tapered fiber, which might not have an expansion of this form. The Mie theory, however, hinges only on the possibility of presenting the *angular* dependence of the incident field as a series of spherical harmonics, which is always possible. The remaining dependence of the incident field on the radial coordinate can be left arbitrary. In this article we assume that this field is such that in the absence of the defect, it excites a single WGM in the resonator. This means that we only need to consider a single term in Eq. (3) making most of the presented results independent on the exact form of the radial dependence of the incident field. We keep it in the form of Eq. (3) for concreteness and easier comparison with the standard Mie theory.

The total physical field at each point is in general a linear combination of fields associated with each sphere. For the external defect case, there are three distinct regions corresponding to the interior of each of the two spheres (regions I and II, respectively), plus the exterior region (III) in which both spheres are situated. In the case of internal coupling configuration, the same three regions exist, except that the interior of the main sphere excludes the volume occupied by the internal defect. The standard Maxwell boundary conditions are applied at the surfaces of the spheres $r_1 = R_1$ and $r_2 = R_2$ by demanding continuity of the tangential components of the total fields $\mathbf{E}$ and $\mathbf{H}$.

In the case of external coupling, the field in regions I and II is given simply by Eq. (2) for $i = 1,2$, respectively. In region III, the total field in coordinate system O_i, $\mathbf{E}^{(i)}_{\rm III}$, is composed of the incident field and the scattered field from each sphere:

$$\mathbf{E}^{(1,2)}_{\rm III} = \mathbf{E}^{(1,2)}_{\rm inc} + \mathbf{E}^{(1)}_{\rm sc} + \mathbf{E}^{(2)}_{\rm sc}. \quad (4)$$

For the internal coupling case, the field in region II is again given by Eq. (2) for $i = 2$, but the interior of the main sphere, region I, now includes a contribution from the scattered field of the defect:

$$\mathbf{E}^{(1)}_{\rm I} = \mathbf{E}^{(1)}_{\rm int} + \mathbf{E}^{(2)}_{\rm sc}. \quad (5)$$

The field in region III now consists of the incident field and the scattered field of only the main sphere:

$$\mathbf{E}^{(1)}_{\rm III} = \mathbf{E}^{(1)}_{\rm inc} + \mathbf{E}^{(1)}_{\rm sc}. \quad (6)$$

Equations (4) and (5) involve combinations of fields that are referred to different coordinate systems. By utilizing the VSH addition theorem [8,25], the total field can be expressed in a single coordinate system. Each VSH function is expanded in terms of the translation coefficients $A_{m_1,l_1,m_2,l_2}(k,\mathbf{d})$, which connect fields of the same polarization, and $B_{m_1,l_1,m_2,l_2}(k,\mathbf{d})$, which connect fields of different polarization. The translation vector $\mathbf{d} = (d,\theta_t,\phi_t)$ connects the origins of the two systems. The addition theorem simplifies considerably when azimuthal symmetry is present in the system, as in our case where the polar axis of each coordinate system coincides with the line connecting the centers of the spheres. In this case, one only deals with translation vectors $\mathbf{d} = (d,0,0)$ and $\mathbf{d} = (d,\pi,0)$. Consequently, the addition theorem couples fields of different polarizations and different polar numbers, but does not couple different azimuthal components so that the azimuthal number m can be used to classify modes of the system as a whole.

Applying the boundary conditions and making use of the orthogonality of the VSH, one obtains a system of coupled equations for expansion coefficients of the scattered and internal fields. For the external defect, this system of equations is that of the standard Mie theory found in Refs. [13,16,17]. For the internal defect the application of the boundary conditions results in a different set of equations, which we present in Appendix A for the most general case (as well as the standard set of equations for the external defect for easy reference). The general expressions for the translation coefficients are given in Appendix B.

III. DEFECT SCATTERING IN WGM RESONATORS

A. Exact solution for the dipole scatterer

We shall assume that in the absence of a scatterer the incident field would have excited in a microsphere a single WGM of either TM or TE polarization with a given angular number $l = L$, dimensionless vacuum frequency $x^{(0)}_{s,L}$, and width $\gamma^{(0)}_{s,L}$ found from a complex pole of the Mie coefficients $\alpha^{(1)}_L$ (TM polarization) or $\beta^{(1)}_L$ (TE polarization). Note that the effective Mie coefficients $\tilde{\alpha}^{(1)}_L$ and $\tilde{\beta}^{(1)}_L$ which arise for the internal defect case have the same poles (see Appendix A). To mimic the experimental situation of excitation by a tapered fiber, we also assume that this incident field impinges only on the main sphere, so that $\mathbf{E}^{(2)}_{\rm inc} = 0$ and $\mathbf{E}^{(1)}_{\rm inc} = \mathbf{E}_{\rm inc}$. We are interested in the fundamental mode (FM) characterized by a field distribution concentrated in one of the equatorial planes of the sphere with no oscillations in radial and polar directions. In the coordinate system with the polar axis perpendicular to the

plane of the mode ($X'Y'Z'$ axes in Fig. 1) this field distribution is described by a single VSH with $|m| = L$:

$$\mathbf{E}_{\text{inc}}(\mathbf{r}') = E_0 \times \begin{cases} \mathbf{N}^{(1)}_{L,L}(\mathbf{r}') & \text{(TM mode)}, \\ \mathbf{M}^{(1)}_{L,L}(\mathbf{r}') & \text{(TE mode)}. \end{cases} \tag{7}$$

However, as discussed in the previous section, the two-sphere problem is more conveniently described when the fields in the main sphere are expressed in the XYZ system of Fig. 1 whose polar axis passes through the centers of both spheres. The field distribution of the FM in this coordinate system cannot be described as a single VSH, but requires a linear combination of VSH with all $-L \leqslant m \leqslant L$. This representation is found with the help of the rotation transformation properties of the spherical harmonics [8]. If the unprimed system is obtained from the primed through successive rotation by Euler angles α,β,γ (following the conventions of [8]), then the incident field of Eq. (9) for the TM mode is expressed in the unprimed coordinates as

$$\mathbf{E}_{\text{inc}}(\mathbf{r}_1) = E_0 \sum_{m=-L}^{L} D^L_{m,L}(-\gamma, -\beta, -\alpha)\mathbf{N}^{(1)}_{L,m}(\mathbf{r}_1), \tag{8}$$

where $D^L_{m,L}$ are Wigner D functions [8]. TE polarized fields obey the same transformation law. As mentioned, the system possess axial symmetry about the Z axis of the XYZ coordinate system. Several conclusions can be drawn from this fact. First of all, due to this symmetry the azimuthal number m remains a "good quantum number" that can be used to classify the normal modes of the resonator-defect system. It means, in other words, that the interaction only couples modes of resonator and the defect which have the same m. Since the field of the defect is composed of the $|m| \leqslant 1$ dipole modes, it is only these modes of the resonator which will be affected by the interaction. The sub-basis comprising the remaining $2L-1$ components of the resonator do not sense the defect at all, and therefore the scattering expansion coefficients for these components can be simply read off from the single-sphere problem:

$$\begin{aligned} a^{(1)}_{L,m} &= \alpha^{(1)}_L D^L_{m,L}, \quad |m| > 1 \text{ (TM mode)}, \\ b^{(1)}_{L,m} &= \beta^{(1)}_L D^L_{m,L}, \quad |m| > 1 \text{ (TE mode)}, \end{aligned} \tag{9}$$

with respective components of the D functions [Eq. (8)] playing the role of the expansion coefficients of the incident field. An immediate consequence of this observation is that in the presence of the defect, $2L-1$ components of the L mode will resonate at the Mie frequency of the ideal single sphere. Therefore, one of the peaks in the spectrum of the resonator-defect system must correspond to this resonance and its frequency and width should not depend on the position of the defect. This conclusion is in complete agreement with experimental results of Ref. [9].

We now turn to the full quantitative solution for the expansion coefficients. Within the dipole approximation for the defect, these coefficients can be decoupled exactly for both the internal and the external defect cases. The dipole approximation is introduced by setting all coefficients $a^{(2)}_{l,m}$ with $l > 1$ to zero. Formally, this approximation can be justified by considering the asymptotic form of the scattering amplitude of the second sphere for $kR_2 = \rho \ll 1$:

$$\alpha^{(2)}_l(\rho) \approx -\left[1 + i\frac{(2l+1)!!(2l-1)!!}{(l+1)\rho^{2l+1}}\left(\frac{ln_2^2 + l + 1}{n_2^2 - 1}\right)\right]^{-1}. \tag{10}$$

In this limit, $\alpha^{(2)}_l$ decays fast with increasing l, which allows one to safely neglect $\alpha^{(2)}_l$ for all $l > 1$ and set the corresponding $a^{(2)}_{l,m}$ to zero. Note, that in the same approximation the $\beta^{(2)}_l$ coefficients vanish identically, reflecting the pure TM behavior of true dipole radiation. Therefore, TE field coefficients $b^{(2)}_{l,m}$ can also be set to zero. The fact that dipole radiation formally corresponds to a TM field does not mean that a TE mode in the resonator would not interact with the defect. Since the addition theorem couples TE and TM WGMs, both polarizations of the field of the resonator are scattered by the defect. The quantitative characteristics of this interaction, however, will be different for WGMs of different polarization due to different properties of $A_{m_1,l_1,m_2,l_2}(k,\mathbf{d})$ and $B_{m_1,l_1,m_2,l_2}(k,\mathbf{d})$ translation coefficients. This fact is completely lost in phenomenological theories of WGM scattering.

After applying the dipole approximation to system (A1) and (A2) presented in Appendix A, the remaining equations can be solved exactly. The solution for the $a^{(1)}_{l,m}$ coefficients for an external defect with a TM mode in the resonator can be presented in the form

$$\begin{aligned} a^{(1)}_{l,m} = {} & \alpha^{(1)}_L D^L_{m,L}\delta_{l,L} + \alpha^{(1)}_l \alpha^{(1)}_L D^L_{m,L} A^{(3)}_{m,1,m,L}(k, -\mathbf{d}) \\ & \times \frac{\alpha^{(2)}_1 A^{(3)}_{m,l,m,1}(k,\mathbf{d})}{1 - \alpha^{(2)}_1 \sigma}. \end{aligned} \tag{11}$$

The general solution of all coefficients for both internal and external defect cases, for either type of incident field polarization can be understood by giving a physical interpretation to Eq. (11). The first term in this equation describes the response of the resonator in the absence of the defect. The presence of the TM Mie coefficient of the resonator, $\alpha^{(1)}_l$, in the next term indicates that it describes the response of the resonator to the field scattered by the defect. This term is proportional to the field incident on the defect due to scattering of the initial excitation by the resonator, $\alpha^{(1)}_L D^L_{m,L} A^{(3)}_{m,1,m,L}(k, -\mathbf{d})$, presented in the defect-centered coordinate system. The indices L and 1 in the translation coefficient imply that this is the portion of the original L mode contributing to the $l = 1$ dipole mode at the position of the defect. The presence of the "A" (rather than a "B") coefficient denotes that this L mode is of the same polarization as the (necessarily TM) dipole mode of the defect. The term $\alpha^{(2)}_1(1 - \alpha^{(2)}_1\sigma)^{-1} A^{(3)}_{m,l,m,1}(k,\mathbf{d})$ corresponds to the field scattered back to the l mode of the resonator, with a similar interpretation of the translation coefficient. The denominator $(1 - \alpha^{(2)}_1\sigma)$ in this expression is responsible for modification of the resonant frequencies of the resonator-scatterer system.

All coefficients $a^{(1)}_{l,m}$ and $b^{(1)}_{l,m}$, for either type of incident field polarization and defect position (internal and external) can be presented in the similar form. The results are summarized in

TABLE I. Functions $f_1^{(e)}$–$f_5^{(e)}$.

		$f_1^{(e)}$	$f_2^{(e)}$	$f_3^{(e)}$	$f_4^{(e)}$	$f_5^{(e)}$
$a_{l,m}^{(1)}$	TM mode	$\alpha_l^{(1)}$	$\delta_{l,L}$	$\alpha_L^{(1)}$	$U_{m,L}^{(3)}$	$U_{m,l}^{(3)}$
	TE mode	$\alpha_l^{(1)}$	0	$\beta_L^{(1)}$	$V_{m,L}^{(3)}$	$U_{m,l}^{(3)}$
$b_{l,m}^{(1)}$	TM mode	$\beta_l^{(1)}$	0	$\alpha_L^{(1)}$	$U_{m,L}^{(3)}$	$V_{m,l}^{(3)}$
	TE mode	$\beta_l^{(1)}$	$\delta_{l,L}$	$\beta_L^{(1)}$	$V_{m,L}^{(3)}$	$V_{m,l}^{(3)}$

Tables I and II. For an external defect, one has

$$\{a_{l,m}^{(1)}, b_{l,m}^{(1)}\} = D_{m,L}^{L}\left[f_1^{(e)}\right]\left\{\left[f_2^{(e)}\right] + \left[f_3^{(e)}\right]\left[f_4^{(e)}\right]\left[f_5^{(e)}\right]\frac{\alpha_1^{(2)}}{1-\alpha_1^{(2)}\sigma}\right\}, \tag{12}$$

where functions $f_1^{(e)}$ through $f_5^{(e)}$ for both a and b coefficients and for both polarizations of the incident wave are defined in Table I.

Expansion coefficients for an internal defect can be presented as

$$\{a_{l,m}^{(1)}, b_{l,m}^{(1)}\} = D_{m,L}^{L}\left[f_1^{(i)}\right]\left\{\left[f_2^{(i)}\right] + \left[f_3^{(i)}\right]\left[f_4^{(i)}\right]\left[f_5^{(i)}\right]\frac{1}{n_0^2 x_1^2}\frac{\alpha_1^{(2)}}{1-\alpha_1^{(2)}\tilde{\sigma}}\right\}, \tag{13}$$

where fuctions $f_1^{(i)}$ through $f_5^{(i)}$ for both a and b coefficients and for both polarizations of the incident wave are defined in Table II and $x_1 = k_0 R_1$.

When deriving these expressions we have taken into account the symmetry properties of the translation coefficients [26],

$$\begin{aligned} A_{m,1,m,l}^{(j)}(kd,0,0) &= (-1)^{1+l} A_{m,l,m,1}^{(j)}(kd,0,0), \\ B_{m,1,m,l}^{(j)}(kd,0,0) &= (-1)^{l+1} B_{m,l,m,1}^{(j)}(kd,0,0), \end{aligned} \tag{14}$$

and introduced the following quantities:

$$\begin{aligned} U_{m,l}^{(j)} &= (-1)^l A_{m,1,m,l}^{(j)}(\rho,0,0) \\ &= (-1)^l \sqrt{\frac{3}{2}}\left[\sqrt{\frac{(l+1)(l+|m|)}{(2l+1)(|m|+1)}} z_{l-1}^{(j)}(\rho)\right. \\ &\quad \left. + (-1)^m \sqrt{\frac{l(l+1-|m|)}{(2l+1)(1+|m|)}} z_{l+1}^{(j)}(\rho)\right], \end{aligned} \tag{15}$$

TABLE II. Functions $f_1^{(i)}$–$f_5^{(i)}$.

		$f_1^{(i)}$	$f_2^{(i)}$	$f_3^{(i)}$	$f_4^{(i)}$	$f_5^{(i)}$
$a_{l,m}^{(1)}$	TM mode	$\alpha_l^{(1)}$	$\delta_{l,L}$	$n_1/G_{\alpha,L}^{(1)}$	$U_{m,L}^{(1)}$	$U_{m,l}^{(1)}/N_{\alpha,l}^{(1)}$
	TE mode	$\alpha_l^{(1)}$	0	$1/G_{\beta,L}^{(1)}$	$-V_{m,L}^{(1)}$	$U_{m,l}^{(1)}/N_{\alpha,l}^{(1)}$
$b_{l,m}^{(1)}$	TM mode	$\beta_l^{(1)}$	0	$1/G_{\alpha,L}^{(1)}$	$-U_{m,L}^{(1)}$	$V_{m,l}^{(1)}/N_{\beta,l}^{(1)}$
	TE mode	$\beta_l^{(1)}$	$\delta_{l,L}$	$1/(n_1 G_{\beta,L}^{(1)})$	$V_{m,L}^{(1)}$	$V_{m,l}^{(1)}/N_{\beta,l}^{(1)}$

$$V_{m,l}^{(j)} = (-1)^l B_{m,1,m,l}^{(j)}(\rho,0,0) = i(-1)^{l+1}\frac{\sqrt{3}}{2} m\sqrt{2l+1} z_l^{(j)}(\rho). \tag{16}$$

Here radial functions are defined as $z_l^{(1)}(\rho) = j_l(\rho)$ and $z_l^{(3)}(\rho) = h_l^{(1)}(\rho)$. Throughout this article, translation coefficients with $j = 1$ take argument $kd = n_1 k_0 d$, while those with $j = 3$ take argument $kd = n_0 k_0 d$. Both translation coefficients take $m = -1, 0, 1$ and vanish explicitly for $|m| > 1$. Parameters σ in Eq. (12) and $\tilde{\sigma}$ in Eq. (13) are defined as

$$\sigma = \sigma_a - \sigma_b, \quad \tilde{\sigma} = \tilde{\sigma}_a - \tilde{\sigma}_b, \tag{17}$$

where

$$\sigma_a = \sum_\nu \alpha_\nu^{(1)}\left[U_{m,\nu}^{(3)}\right]^2, \tag{18}$$

$$\sigma_b = \sum_\nu \beta_\nu^{(1)}\left[V_{m,\nu}^{(3)}\right]^2, \tag{19}$$

$$\tilde{\sigma}_a = \sum_\nu \tilde{\alpha}_\nu^{(1)}\left[U_{m,\nu}^{(1)}\right]^2, \tag{20}$$

$$\tilde{\sigma}_b = \sum_\nu \tilde{\beta}_\nu^{(1)}\left[V_{m,\nu}^{(1)}\right]^2. \tag{21}$$

Equations (12) and (13) completely characterize the scattered field of the main sphere. For the external defect case, the total external field includes a contribution from the dipole scatterer itself, whose single coefficient $a_{1,m}^{(2)}$ is, for TM and TE excitations, respectively:

$$a_{1,m}^{(2)} = \frac{D_{m,L}^{L}\alpha_1^{(2)}}{1-\alpha_1^{(2)}\sigma} \times \begin{cases} -\alpha_L^{(1)} U_{m,l}^{(3)} & \text{(TM mode)}, \\ \beta_L^{(1)} V_{m,l}^{(3)} & \text{(TE mode)}. \end{cases} \tag{22}$$

The validity of the solutions presented relies on the convergence of the infinite sums appearing in the definition of σ and $\tilde{\sigma}$, which is not trivial since spherical Hankel functions entering these sums increase with increasing polar number l. Considering the asymptotic forms of the spherical Hankel functions of the first kind $h_l^{(1)}(\rho)$ in the limit $l \to \infty$, ρ fixed [27], we can show that the terms in these sums behave in the limit of large l as

$$\lim_{l\to\infty}\left\{\begin{matrix} \alpha_\nu^{(1)}\left[U_{m,\nu}^{(3)}\right]^2 \\ \tilde{\alpha}_\nu^{(1)}\left[U_{m,\nu}^{(1)}\right]^2 \end{matrix}\right\} = \frac{3}{2} i\left(1-\frac{m^2}{2}\right)\frac{1-n_1^2}{1+n_1^2}\frac{\nu^2}{(kd)^3} \times \left\{\begin{matrix} (R_1/d)^{2\nu+1} \\ -n_1^{-3}(d/R_1)^{2\nu+1} \end{matrix}\right\}. \tag{23}$$

Equation (23) proves the required convergence, given that d is always less than R_1 for internal defects, and always greater than R_1 for external defects. Cross-polarization parameters σ_b and $\tilde{\sigma}_b$ converge much faster, independent of the translation distance. This reflects the fact that translation does not couple high-order multipoles of different polarizations, since the fields $\mathbf{N}_{l,m}$ and $\mathbf{M}_{l,m}$ have pure radial or pure circulatory polarization for $l \to \infty$.

We have shown that the problem of interaction between a WGM of a spherical resonator and a dipole has an exact solution, so that the expansion coefficients of the field in different spatial regions of this system can be obtained analytically in the explicit form. In the next section of the

article we analyze the obtained solutions in the vicinity of the defect-induced resonances.

B. Defect-induced resonances

Resonances are found by examining the behavior of the expansion coefficients in a frequency range close to the ideal Mie resonance with $l = L$. The most important quantities for this analysis are σ and $\tilde{\sigma}$ appearing in the denominator of Eqs. (12) and (13) and defined in Eq. (17). If the $l = L$ resonance is well separated from other resonances so that in its vicinity no WGMs with $l \neq L$ have their own resonances, we can assume that the largest contribution to σ and $\tilde{\sigma}$ comes from the terms which contain resonant scattering amplitudes $\alpha_L^{(1)}$ and $\tilde{\alpha}_L^{(1)}$ (for TM excitations) or $\beta_L^{(1)}$ and $\tilde{\beta}_L^{(1)}$ (TE excitations). Separating these terms out we define reduced sums σ' and $\tilde{\sigma}'$ such that for an external defect and a TM polarized mode we have

$$\sigma' = \left\{\sigma_a - \alpha_L^{(1)}\left[U_{m,L}^{(3)}\right]^2\right\} - \sigma_b, \tag{24}$$

with the similar definition for the other cases. With this modification, coefficients $a_{l,m}^{(1)}$ for the case of the external defect for a TM excitation can be presented as

$$a_{l,m}^{(1)} = \begin{cases} \dfrac{D_{m,L}^{L}\left[1-\alpha_1^{(2)}\sigma'\right]}{\left[\alpha_L^{(1)}\right]^{-1}\left[1-\alpha_1^{(2)}\sigma'\right]-\alpha_1^{(2)}\left[U_{m,L}^{(3)}\right]^2} & l = L, \quad |m| \leqslant 1, \qquad (25a) \\ \dfrac{D_{m,L}^{L}\alpha_l^{(1)}\alpha_1^{(2)}U_{m,L}^{(3)}U_{m,l}^{(3)}}{\left[\alpha_L^{(1)}\right]^{-1}\left[1-\alpha_1^{(2)}\sigma'\right]-\alpha_1^{(2)}\left[U_{m,L}^{(3)}\right]^2} & l \neq L, \quad |m| \leqslant 1, \qquad (25b) \\ \alpha_l^{(1)}D_{m,L}^{L}\delta_{l,L} & |m| > 1, \qquad (25c) \end{cases}$$

while for the internal defect they take the form

$$a_{l,m}^{(1)} = \begin{cases} \dfrac{1}{\tilde{N}_{\alpha,L}^{(1)}}\dfrac{D_{m,L}^{L}\left\{\lambda_L\alpha_1^{(2)}\left[U_{m,L}^{(1)}\right]^2+N_{\alpha,L}^{(1)}\left[1-\alpha_1^{(2)}\tilde{\sigma}'\right]\right\}}{\left[\tilde{\alpha}_L^{(1)}\right]^{-1}\left[1-\alpha_1^{(2)}\tilde{\sigma}'\right]-\alpha_1^{(2)}\left[U_{m,L}^{(1)}\right]^2} & l = L, \quad |m| \leqslant 1, \qquad (26a) \\ \dfrac{n_1}{x_1^2G_{\alpha,l}^{(1)}\tilde{N}_{\alpha,L}^{(1)}}\dfrac{D_{m,L}^{L}\alpha_1^{(2)}U_{m,L}^{(1)}U_{m,l}^{(1)}}{\left[\tilde{\alpha}_L^{(1)}\right]^{-1}\left[1-\alpha_1^{(2)}\tilde{\sigma}'\right]-\alpha_1^{(2)}\left[U_{m,L}^{(1)}\right]^2} & l \neq L, \quad |m| \leqslant 1, \qquad (26b) \\ \alpha_l^{(1)}D_{m,L}^{L}\delta_{l,L} & |m| > 1, \qquad (26c) \end{cases}$$

The preceding formulas demonstrate that both internal and external defect cases result in a breaking of the degeneracy of the azimuthal components, and, as discussed in what follows, resonant behavior. The $b_{l,m}^{(1)}$ coefficients, as well as both coefficients for the case of a TE excitation, take an analogous form. The degeneracy breaking is evidenced by the three distinct groups of coefficients in these equations. First, for $|m| > 1$ all translation coefficients vanish and we recover the single-sphere case as it was anticipated on the basis of the symmetry arguments. Coefficients with $l = L$ describe modification of the initial FM by its interaction with the defect. Finally, coefficients for $l \neq L$ and $|m| < 1$ describe scattering-induced intermode coupling.

In the vicinity of a single-sphere resonance, Mie coefficients α_L and β_L can be presented in the form of a complex Lorentzian:

$$\alpha_L^{(1)}(z) \approx \frac{-i\gamma_{s,L}^{(0)}}{z - x_{s,L}^{(0)} + i\gamma_{s,L}^{(0)}}. \tag{27}$$

The modified Mie parameters $\tilde{\alpha}_L$ and $\tilde{\beta}_L$ can be presented in a similar form differing only by an overall factor. Since $\gamma_{s,L}^{(0)}$ is very small for WGMs, the Mie parameters are the fastest-changing quantities in Eqs. (25) and (26). Therefore, using Eq. (27), and calculating all other quantities at $x = x_L^{(0)}$, we can present the coefficients $a_{l,m}^{(1)}$ and $b_{l,m}^{(1)}$ in the Lorentzian form with new poles $z_{L,m} = x_{L,m} - i\gamma_{L,m}$ (the radial index s has been suppressed for brevity). For externally positioned defects, the poles are

$$z_{L,m} = x_L^{(0)} - i\gamma_L^{(0)} - i\gamma_L^{(0)}\frac{\alpha_1^{(2)}}{1-\alpha_1^{(2)}\sigma'} \times \begin{cases} \left[U_{m,L}^{(3)}\right]^2 & \text{(TM mode)}, \\ -\left[V_{m,L}^{(3)}\right]^2 & \text{(TE mode)}, \end{cases} \tag{28}$$

whereas for internal defects, one has

$$z_{L,m} = x_L^{(0)} - i\gamma_L^{(0)} - i\gamma_L^{(0)}\frac{\alpha_1^{(2)}}{1-\alpha_1^{(2)}\tilde{\sigma}'} \times \begin{cases} \left[\tilde{N}_{\alpha,L}^{(1)}/N_{\alpha,L}^{(1)}\right]\left[U_{m,L}^{(1)}\right]^2 & \text{(TM mode)}, \\ -\left[\tilde{N}_{\beta,L}^{(1)}/N_{\beta,L}^{(1)}\right]\left[V_{m,L}^{(1)}\right]^2 & \text{(TM mode)}. \end{cases} \tag{29}$$

Separation of the real and imaginary parts of the last terms in Eqs. (28) and (29) gives the frequency shifts and broadenings induced by interaction with the defect.

For a given set of experimental parameters n_0, n_1, n_2, R_1, R_2, D, and L, there are different resonances $z_{L,m}$ for the different values of m. The number of these resonances is determined by the m dependence of $U^{(j)}_{m,l}$ and $V^{(j)}_{m,l}$. Both functions vanish for $|m| > 1$, giving the standard Mie resonance. $U^{(j)}_{m,l}$ can take $m = 0$ or $|m| = 1$, while $V^{(j)}_{m,l}$ vanishes for $m = 0$, and its square, $[V^{(j)}_{m,l}]^2$, is identical for $m = \pm 1$. Thus, for TM modes there are two additional defect-induced resonances, while for TE modes there is one. Combining this with the response at the single-sphere frequency for $|m| > 1$, we see that instead of a simple doublet our theory predicts either two or three peaks based on the polarization of the incident mode.

Another qualitative feature of the resonance conditions Eqs. (12) and (13) is that they do not contain the $D^L_{m,L}(-\gamma,-\beta,-\alpha)$ and are therefore independent of the the angular position of the defect. Thus, a change in the angular position of a defect does not change the position or width of the resonance. However, the appearance of $D^L_{m,L}(-\gamma,-\beta,-\alpha)$ in the numerator of Eq. (25) results in a dependence of the amplitude of the resonance on the angular coordinates of the defect, which is due to the longitudinal and latitudinal phase oscillations of the excited mode. On the other hand, a change in the defect's radial distance from the resonator always leads to a change in the resonant frequency. The assumption that intensity oscillations correspond to resonant frequency shifts was taken in Ref. [9] as confirmation of the backscattering paradigm. In fact, it is seen here that the amplitude and frequency of a resonance can be altered independently.

If one neglects the small contribution from nonresonant modes [terms σ' and $\tilde{\sigma}'$ in Eqs. (25) and (26)], the defect-modified resonance frequencies can be found as

$$z_{L,m} = x^{(0)}_L(1 - \delta x_{L,m}) - i\gamma^{(0)}_L(1 + \delta\gamma_{L,m}), \tag{30}$$

where

$$\begin{aligned} \delta x_{L,m} &= \gamma^{(0)}_L \frac{p\left[x^{(0)}_L\right]}{R_1^2 d} F, \\ \delta\gamma_{L,m} &= \frac{2}{3}\frac{p^2\left[x^{(0)}_L\right]^5}{R_1^5 d} F, \end{aligned} \tag{31}$$

and

$$F = \begin{cases} \psi^{(e)}_{L,m}\left[n_0 k^{(0)}_{s,L} d\right] & \text{(TM, external)}, \\ \left\{g^{(e)}_L\left[n_0 k^{(0)}_{s,L} d\right]\right\}^2 & \text{(TE, external)}, \\ \mathrm{Re}\left[\frac{\tilde{N}^1_{\alpha,L}}{N^1_{\alpha,L}}\right] \psi^{(i)}_{L,m}\left[n_1 k^{(0)}_{s,L} d\right] & \text{(TM, internal)}, \\ \mathrm{Re}\left[\frac{\tilde{N}^1_{\beta,L}}{N^1_{\beta,L}}\right] \left\{g^{(i)}_L\left[n_1 k^{(0)}_{s,L} d\right]\right\}^2 & \text{(TE, internal)}. \end{cases} \tag{32}$$

Parameter

$$p = \frac{n^2_{\mathrm{rel}} - 1}{n^2_{\mathrm{rel}} + 2}\left(\frac{n_2}{n_{\mathrm{rel}}} R_2\right)^3 \tag{33}$$

is the polarizability of a dielectric sphere, with $n_{\mathrm{rel}} = n_2/n_0$ for the external case, and $n_{\mathrm{rel}} = n_2/n_1$ for the internal case. The functions $g^{(e,i)}_L$ and $\psi^{(e,i)}_{L,m}$ describe the dependence of the defect-induced resonance shift and broadening upon the position of the defect and the azimuthal number. They are defined as

$$\psi^{(e,i)}_{L,m}(\rho) = \frac{1}{2L+1}\left[(-1)^m\sqrt{\frac{(L+1)(L+m^2)}{(L-1/2)(1+m^2)}}\, g^{(e,i)}_{L-1}(\rho) + \sqrt{\frac{L(L+1-m^2)}{(L+3/2)(1+m^2)}}\, g^{(e,i)}_{L+1}(\rho)\right]^2, \tag{34}$$

$$g^{(e)}_L(\rho) = \frac{1}{\sqrt{q}}\exp\{\nu[\mathrm{arctanh}(q) - q]\},$$

$$q = \sqrt{1 - \left(\frac{\rho}{\nu}\right)^2}, \quad \nu = L + \frac{1}{2},$$

$$g^{(i)}_L(\rho) = \frac{1}{\sqrt{w}}\cos\{\nu[w - \mathrm{arcsec}(\rho/\nu)] - \pi/4\},$$

$$w = \sqrt{\left(\frac{\rho}{\nu}\right)^2 - 1}, \quad \nu = L + \frac{1}{2}.$$

Here the functions $g^{(e,i)}_L(\rho)$ are derived from the asymptotic forms of radial functions for $L \gg 1$ in the region of interest, $\rho/L < 1$ and $\rho/L > 1$ for the external and internal cases, respectively. All functions $g^{(i)}_L[n_1 k^{(0)}_{s,L} d]$, $g^{(e)}_L[n_0 k^{(0)}_{s,L} d]$, $\psi^{(i)}_{L,m}[n_1 k^{(0)}_{s,L} d]$, and $\psi^{(e)}_{L,m}[n_0 k^{(0)}_{s,L} d]$ are positive definite so that the sign of the shift of the resonance is determined solely by the polarizability of the defect, with red shifts for scatterers with $n_{\mathrm{rel}} > 1$ and blue shifts for $n_{\mathrm{rel}} < 1$. However, the precise asymptotic behavior of functions is different, which translates into a different dependence of the frequency shifts and broadenings of the resonances upon defect distance d.

It is instructive to compare our predictions for the frequency shift and broadening of the defect-induced resonances with those obtained in Ref. [9]. While the phenomenological approach employed in Ref. [9] is not capable of predicting the actual dependence of these quantities upon the defect position and cannot distinguish between TM and TE polarizations or predict the existence of the third peak for TM excitation, it does reproduce certain features of our solution. For instance, it captures the respective linear dependence of the frequency shift and the quadratic dependence of the broadening on the polarizability of the defect, as well as the fact that both the shift and the broadening are determined by the same function of the defect's position. At the same time, while Mazzei *et al.* predict linear and fourth-power dependence of the frequency shift and the broadening on the frequency of the resonance, respectively, our calculations give for these quantities, respectively, $[x^{(0)}_L]^2$ and $[x^{(0)}_L]^5$ dependencies multiplied by some slower changing functions. The discrepancy can be traced to different asymptotic properties of WGMs in the evanescent and propagating regions: Had we used the asymptotic expansions of the Hankel functions for the latter region instead of former, our formulas would yield the same power laws as the phenomenological theory.

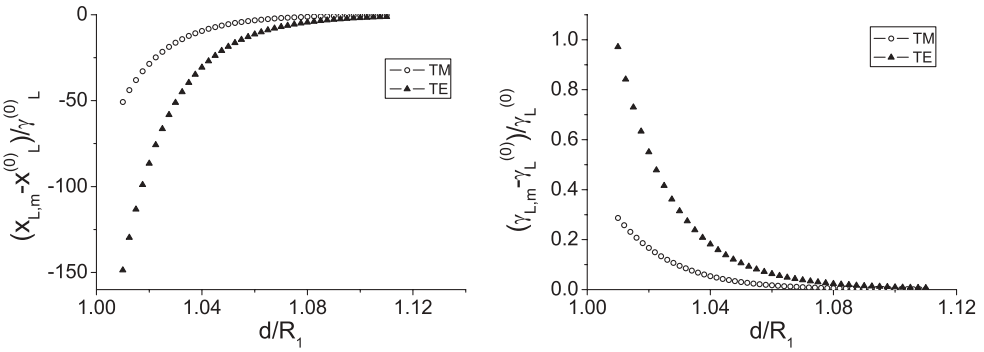

FIG. 2. Frequency shift (left) and broadening (right) of the $|m| = 1$ resonance for an external defect with $L = 39$ for both TM and TE polarization.

Equation (31) has been obtained in what we call the "resonance approximation," which neglects the reduced sums σ' and $\tilde{\sigma}'$ in Eqs. (28) and (29) containing contributions from all terms with $l \neq L$. This is equivalent to neglecting intermode coupling, since both the reduced sums and nonresonant mode expansion coefficients vanish when we disregard nonresonant Mie parameters. Analysis of these terms summarized in Eq. (23) shows convergence of the series, but it also shows that for the defect positioned very close to the surface of the main sphere, this convergence can be rather slow, and the contribution of σ' and $\tilde{\sigma}'$ can be appreciable. With σ' and $\tilde{\sigma}'$ taken into account, the expressions for defect-induced frequencies still can be presented in the same form as Eq. (31). The coupling to nonresonant high-l modes manifests itself as a renormalization of the defect's dipole polarization: Instead of the standard Eq. (33), this parameter takes the form

$$p_{\text{eff}} = p_0 \left\{ 1 + p_0 \frac{2[x_L^{(0)}]^3}{3R_1^3} \text{Im}[\sigma] \right\}^{-1}, \tag{35}$$

where p_0 is defined by Eq. (33), and we have neglected a small real part of σ. The most significant consequence of this renormalization is the dependence of the polarizability on the position of the defect. This reflects the fact that the field which polarizes the defect (i.e., the scattered field of the resonator) is itself strongly dependent on the position of the defect. One can recall in this context a modification of quasistatic polarizability of a dipole placed near a plane dielectric surface, which is described by an expression similar to Eq. (35) with $\text{Im}\sigma \propto 1/z^3$, where z is the distance between the dipole and the surface [28]. It should be understood, however, that in spite of the formal analogy, the nature of the effect considered here is essentially different. Indeed, in the static case the renormalization is caused by interaction between the dipole and the electrostatic field of its image, while for the situation considered here it is mainly due to interaction of the dipole with the evanescent fields of the high-order WGMs.

IV. NUMERICAL EXAMPLE AND DISCUSSION

In order to illustrate the general results obtained and discuss their experimental implications, we calculated various physical quantities for the particular case of the TM mode $L = 39$ with $n_1 = 1.59$, which corresponds to an experimental situation considered in Ref. [29]. We choose the external defect to have the same refractive index $n_2 = 1.59$ and radius $R_2/R_1 = 0.008$, while the internal defect is modeled as a vacuum cavity with $n_2 = 1$ and the same radius. Both are positioned in the plane of the fundamental mode, where the interaction strength is strongest. These calculations require truncation of two types of infinite sums: first, the σ or $\tilde{\sigma}$, which appear in the denominators of Eqs. (12), (13), and (22) for the expansion coefficients, and second, the overall summation of VSH over mode number l, required for the evaluation of the field itself. By checking convergency of the sums, we determined that a reasonable accuracy for all calculated quantities is obtained when both sums are truncated at $l_{\max} = 60$.

We begin by presenting dependence of frequency shifts and broadening of the defect-induced resonances versus defect position. For external defects, the functions $\{g_L^{(e)}[n_0 k_{s,L}^{(0)} d]\}^2$ and $\psi_{L,m}^{(e)}[n_0 k_{s,L}^{(0)} d]$, appearing in Eqs. (34) and (35), are monotonically decreasing with d, resulting in smaller shifts and broadening at larger distances. This reflects the weakening of the interaction as the external defect is removed from the evanescent field concentrated at the surface of the sphere. This behavior is demonstrated in Fig. 2, where we have plotted relative frequency shift and broadening vs defect distance for the $|m| = 1$ induced resonance for both the TM and the TE polarized modes. It is interesting to note that the scattering is stronger for TE-polarized modes as evidenced by the frequency shift and broadening.

For internal defects, the internal field of the resonator is strongly nonmonotonous with a sharp peak slightly away from the surface. This field also behaves differently for $m = 0$ and $m = \pm 1$ azimuthal components. As a result, the distance dependence of the spectral characteristics of the internal defect system is more complex, as it can be different for different resonances and is also nonmonotonic. These properties can also be illustrated by the radiative power spectrum of the sphere-defect system, which we calculate by integrating the Poynting vector of the total scattered field in the far zone. The results of these calculations for TM excitation are shown in Fig. 3 for different defect distances d. One can see that for both defect configurations the $m = 0$ resonance is shifted further from $x_L^{(0)}$ and is weaker than the $m = \pm 1$ resonance, signifying a much stronger interaction between

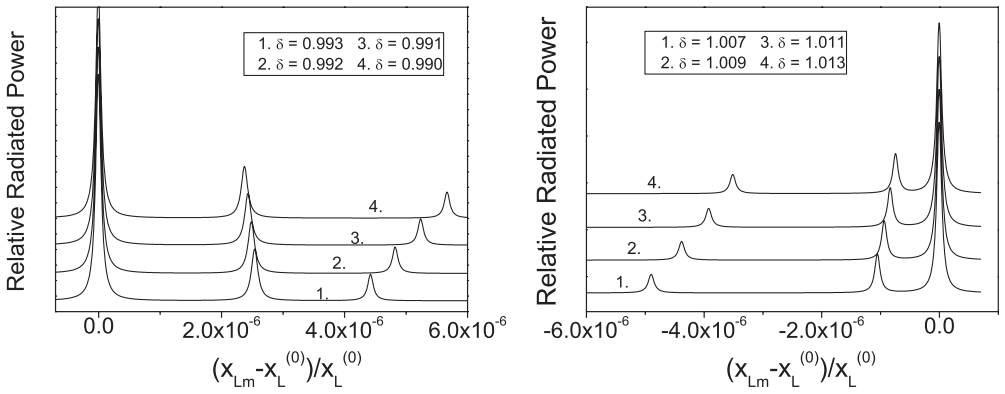

FIG. 3. Radiated power of the microsphere-defect system with varying distance $\delta = d/R_1$ for the internal (left) and external (right) defect cases. The plots are scaled relative to the power radiated by the ideal resonator at the ideal Mie frequency.

the defect and the sphere for the mode with $m = 0$ than for modes with $|m| = 1$. The $m = 0$ mode corresponds to the orientation of the dipole moment of the defect along the Z axis of the coordinate system, while for $m = \pm 1$ modes this dipole moment lies in the XY plane. Therefore, the difference between these two cases reflects the dependence of the interaction strength between the electric field and the dipole upon the orientation of the latter. This is one of the main factors overlooked by the traditional backscattering approach. This also explains why a TE polarized WGM, which has no radially outward component, gives rise to only the $|m| = 1$ resonance. The $m = 0$ peak is only found in TM polarized WGMs, and its weakness makes it more difficult for experimental identification. We suggest, therefore, that the experimentally observed spectral doublets correspond to the original single-sphere resonance and the $m = \pm 1$ resonance introduced by the defect. The presence of the third peak can still be confirmed in an experiment with the controlled scattering of the type carried out in Ref. [9], but covering a broader spectral range. This search might be complicated by the fact that the real microresonators are not ideal spheres so that their spectra contain many more spectral lines due to lifting of the degeneracy of the WGMs. In order to identify the additional defect related spectral feature in this situation, one would have to purposefully study modifications of the spectrum caused by changing the position of the scatterer.

The presented plots also demonstrate a significant difference between the internal and the external defects. The most obvious of them is the difference in the sign of the frequency shift (redshift for external defect and blueshift for the external defect) caused by the difference in the relative refractive index of the defect for these two configurations. More fundamental is the difference in dependence of the magnitudes of the shifts upon the defect distance d. The monotonous decrease in the shift and broadening for both resonances of the external defect reflects the evanescent nature of the field outside of the resonator. In the case of the internal defect, the $m = 0$ and $|m| = 1$ resonances demonstrate opposite behavior: As the defect is moved inward, away from the surface, the $|m| = 1$ peak moves closer to the single-sphere resonance, while the $m = 0$ peak is pushed farther away. Since the magnitude of the shift is a measure of the strength of interaction, this behavior can be explained by examining the intensity of the field that interacts with the defect. Figure 4 plots field intensity of the $m = 0$ mode and the sum of intensities of modes with $m = \pm 1$ as functions of the radial coordinate at the angular position of the defect's center. This figure shows that farther away from the surface the $|m| = 1$ field decreases and the $m = 0$ field becomes stronger, in agreement with the behavior of the resonance frequency shifts. One can predict that moving the defect even further toward the sphere's center will result in nonmonotonic behavior of the $m = 0$ peak, which will begin moving backward toward the unperturbed single-sphere resonance.

Another important characteristic of the scattered field is the directional dependence of its intensity. It is more convenient

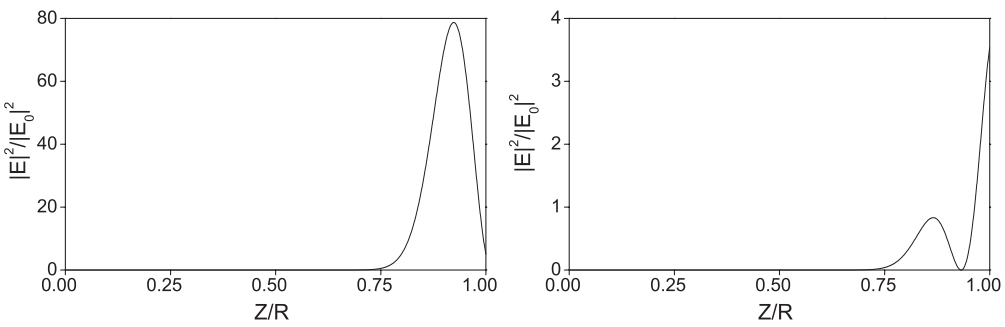

FIG. 4. Field intensity in the radial direction of the unperturbed $m = 0$ (left) and $|m| = 1$ (right) modes.

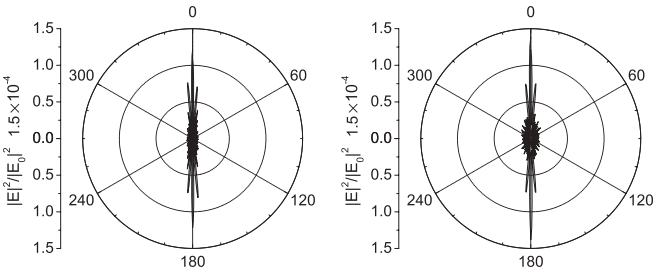

FIG. 5. Directional plot of the radiated energy in the far field for internal (left) and external (right) defect cases.

to describe this dependence using the $X'Y'Z'$ coordinate system, whose equatorial plane coincides with the plane of the initially excited FM. The dependence of the intensity upon azimuthal angle ϕ' of this coordinate system in its equatorial plane calculated for the $|m| = 1$ defect-induced resonance is shown in Fig. 5. In these simulations the defect was placed directly at the surface of the larger sphere for both internal and external configurations, and the intensity was calculated in the far-field region. One can see that there is a drastic increase in the field intensity along the line that bisects the plane of the larger sphere and intersects the defect, resulting in strong directionality of the scattering. A similar effect of defect-induced directionality of scattering in two-dimensional microdisk resonators was discussed recently in Ref. [30]. The fundamental cause of this effect is similar for both defect configurations: The shift of the resonance frequency of $|m| = 1$ azimuthal components results in selective excitation of these particular modes at the respective frequencies. As a result, the scattered field pattern is also very close to that of an ideal sphere with two $m = \pm 1$ modes excited simultaneously. This assertion can be verified by comparing Fig. 5 with Fig. 6, where the scattering intensity calculated for the latter situation is presented.

The directional dependence of the intensity of the scattered field can be related to the spatial distribution of the internal field of the microsphere. To find this distribution, one can use coefficients of the scattered field in combination with original coupled equations to calculate the expansion coefficients of the internal field. Figure 7 plots the surface field intensity in the plane of the WGM for the external defect (the internal defect yields a very similar plot). At the frequency of the $|m| = 1$ defect-induced peak, the field profile demonstrates $2L$

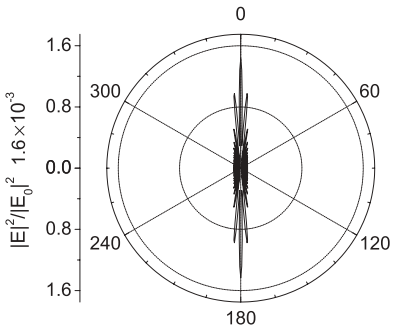

FIG. 6. Scattered field of two $m = \pm 1$ modes excited in a single ideal sphere.

oscillations and a drastic increase in intensity in the vicinity of the defect, which also manifests itself in the far field. At the frequency of the single-sphere resonance the situation is reversed: There are $2L$ oscillations which are phase shifted compared to the defect-induced resonance and are accompanied by a significant decrease in the field's intensity in the defect's proximity. Figure 7 is again explained by the fact that the field at the defect-induced resonance is mainly composed of the m components with $|m| = 1$. The field of these WGMs is characterized by $L - |m| + 1 = L$ oscillations for θ changing between 0 and π, giving their total number equal to $2L$. These modes are also characterized by the enhancement of the field in the vicinity of $\theta = 0$, which explains a drastic rise in the intensity around the location of the defect. The field distribution at the single-sphere resonance can be understood by noting that this field is composed of modes with $|m| > 1$, which when added to the remaining $|m| \leqslant 1$ components would have produced a flat distribution of the intensity. Therefore, removal of these components obviously results in the decrease of the field around the defect and phase-shifted oscillations elsewhere.

We complete our discussion of optical properties of the resonator-defect system with a brief analysis of the defect-induced coupling between modes with different polar numbers l of the same or different polarizations. The latter constitutes the effect of cross-polarization scattering. Quantitative and qualitative significance of these effects are strongly dependent on the parameters of the particular structure and the polar number of the excited mode. In the case considered here, the $L = 39$ TM mode is spectrally separated from other TM and TE modes, and therefore one should expect that intermode and cross-polarization scattering to be small. Indeed, our calculations of the scattered and internal TM fields show that all qualitative effects are described by considering only $l = L$ terms. Nevertheless, taking into account the intermode coupling is still essential for obtaining accurate quantitative results. If, however, one or several TM modes overlap spectrally with the main excited mode, which might be possible for larger values of L, one can expect significant qualitative effects due to intermode coupling. Cross-polarization scattering in the situation under consideration is a more experimentally significant effect because it is observable even with a calculated conversion efficiency of about 5%. Moreover, we found that by increasing the size of the defect one can achieve a more significant polarization conversion while remaining within the range of applicability of the dipole approximation. This situation is illustrated in Fig. 8, where we present the spectrum of the sum of squared absolute values of the TE coefficients characterizing the scattered field due to cross polarization in comparison with the respective quantity for the $l \neq L$ modes of TM polarization. These plots show the spectrum in the vicinity of the $|m| = 1$ resonance at two distances. One can see that the polarization conversion is comparable with, and, for the internal defect, even exceeds the contribution from the nonresonant TM modes. We also note that at the second of the defect-induced resonances ($m = 0$), there is no contribution from TE modes, due to vanishing of cross-polarization translation coefficients $B^{(j)}_{0,l',0,l}$. This effect might aid in experimental identification of the $m = 0$ resonance

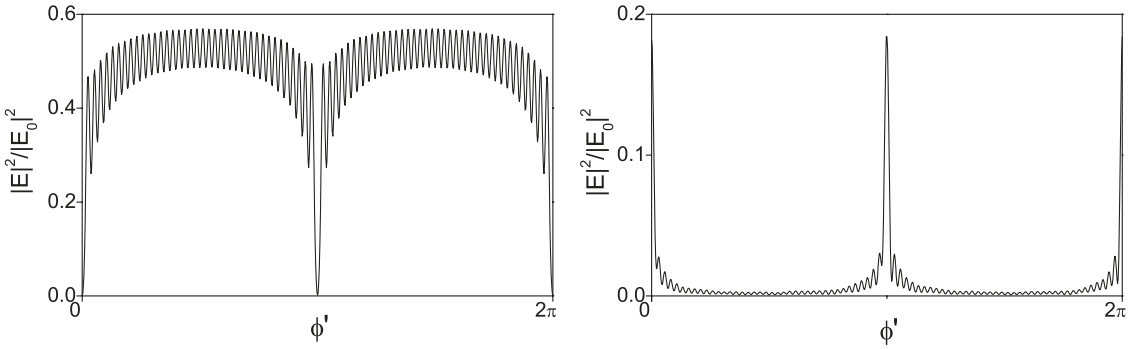

FIG. 7. Variation of the surface field intensity with azimuthal coordinate in the primed system (ϕ') at the frequency of ideal Mie resonance (left) and the defect-induced resonance (right).

by considering polarization-resolved spectra. The $|m| = 1$ resonance will be characterized by a peak in both TM and TE spectra, while the $m = 0$ resonance will only have a peak in the TM spectrum.

Finally, we comment on the relation between our results and the multidefect problem. In the approximation of noninteracting defects, the field in the presence of multiple defects is a sum of fields due to each defect separately. Therefore, the generalization of these results would include finding the field distribution for a generic position of the defect and averaging it over different a defect's coordinates. However, since the interaction with each defect can be considered independently, we can always analyze each one in a coordinate system with its polar axis passing through the centers of the defect and the main sphere. Therefore, since we are free to specify an arbitrary inclination of the defect with respect to the plane of the incident mode (by way of the Euler angles in $D^L_{m,L}$), the results obtained here can be directly used to analyze the multidefect case. If all defects are identical and positioned at the same distances from the center of the main sphere, the position and the width of the defect-induced resonances will remain the same as in the single-defect case. However, the fluctuations in size and position of the defects will introduce additional shifts and inhomogeneous broadening of the resulting peaks. A more detailed account of the extension of the results obtained here to the multidefect case will be given in a subsequent presentation.

V. CONCLUSION

The theory presented here gives a complete solution to the problem of scattering of WGMs of a spherical microresonator due to a single dipole defect. The treatment is based on a presentation of a defect as a small sphere and solving the resulting two-sphere problem. The latter has been generalized compared to previous works to include the case of a smaller sphere situated inside of a larger sphere. This situation takes into account a possibility of internal defects, which can appear either spontaneously during a fabrication process or be introduced deliberately. In both external- and internal-defect cases, the two-sphere Mie theory is shown to yield a closed-form analytical solution for modal expansion coefficients of the electromagnetic field. The developed theory successfully explains all salient experimental results on an *ab initio* basis without recourse to any ad hoc assumptions. Moreover, this theory shows that the currently accepted paradigm of WGM scattering based on the backscattering hypothesis is incomplete and misses important features of the phenomenon under consideration. Instead, we offer a transparent physical picture of this effect based on consideration of normal modes of the sphere-defect system.

In addition to providing exact expressions for defect-induced shifts and broadening of experimentally observed peaks, the theory predicts a number of new phenomena. In particular, we show that WGMs of TE and TM polarizations

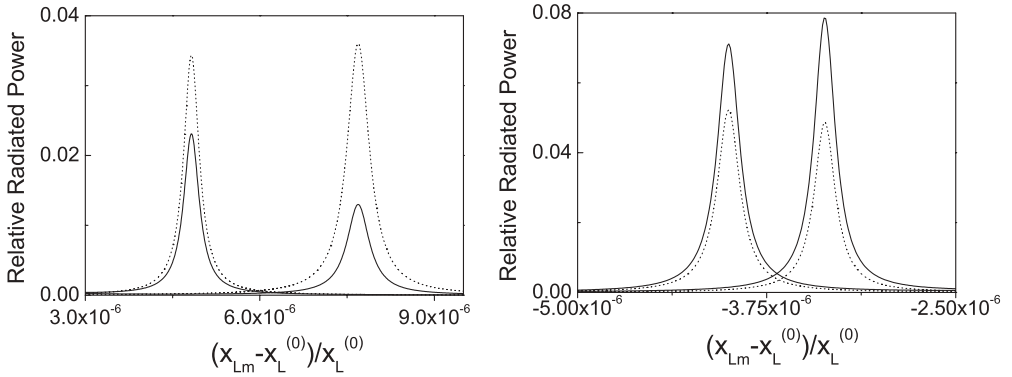

FIG. 8. Individual radiation contributions from TM (solid lines) and TE (dotted lines) modes for internal (left panel) and external (right panel) defects for the $|m| = 1$ resonance at two difference distances. The spectra are scaled relative to the power radiated by the ideal resonator at the ideal Mie frequency.

interact with defects differently. In particular, TE WGMs give rise to only one defect-induced resonance, which in combination with the unaffected single-sphere resonance yields a spectral doublet. At the same time TM modes produce two defect-induced resonances, giving rise to a triplet of peaks. This polarization dependence of the scattering can be used to observe and identify the predicted third peak. Furthermore, the theory predicts defect-induced cross-polarization scattering, which is shown to depend strongly on the parameters of the system under consideration and can be a significant effect.

The predictions of our theory concerning the details of the frequencies and broadening of the defect-induced resonances can also be verified experimentally. For instance, it would be interesting to compare the position dependencies of these quantities shown in Fig. 2 with the results of Ref. [9]. In addition, the authors of Ref. [31] used the results of Ref. [9] to determine the size distribution of nanoparticles by their effect on WGM resonances. Our predictions for these quantities [Eq. (31)] differ significantly from those of Ref. [9] (see more details in Sec. III B). As a result, the size distributions obtained on the basis of the results of this article may deviate from those derived from results of Ref. [9]. By performing experiments similar to that in Ref. [31] and utilizing particles with known size distribution, this distinction might be observed.

ACKNOWLEDGMENTS

One of the authors (L.D.) thanks T. Pertsch and A. Chipouline from F. Schiller University, Jena, Germany, for their hospitality during L.D.'s visit, where part of this work was performed, and multiple useful discussions. Financial support by AFOSR via Grant No. FA9550-07-1-0391 and support by PCS-CUNY grants are acknowledged.

APPENDIX A: EQUATIONS FOR FIELD EXPANSION COEFFICIENTS

In the case when a defect is positioned outside of the resonator, the application of Maxwell boundary conditions results in a standard set of equations for the field-expansion coefficients, which we present here for completeness:

$$a_{l,m}^{(1,2)} = \alpha_l^{(1,2)} \left\{ \eta_{l,m}^{(1,2)} + \sum_\nu \left[a_{\nu,m}^{(2,1)} A_{m,\nu,m,l}^{(3)}(k,\mathbf{d}_{1,2}) + b_{\nu,m}^{(2,1)} B_{m,\nu,m,l}^{(3)}(k,\mathbf{d}_{1,2}) \right] \right\}, \tag{A1}$$

$$b_{l,m}^{(1,2)} = \beta_l^{(1,2)} \left\{ \zeta_{l,m}^{(1,2)} + \sum_\nu \left[b_{\nu,m}^{(2,1)} A_{m,\nu,m,l}^{(3)}(k,\mathbf{d}_{1,2}) + a_{\nu,m}^{(2,1)} B_{m,\nu,m,l}^{(3)}(k,\mathbf{d}_{1,2}) \right] \right\}. \tag{A2}$$

After applying the dipole approximation, $a_{l,m}^{(2)} = 0$ for $l > 1$ and $b_{l,m}^{(2)} = 0$, the remaining set of equations can be solved exactly to give the results presented in Eqs. (11) and (12).

Application of MSMT to the situation where a small sphere is completely surrounded nonconcentrically by a larger sphere leads to a different system of equations connecting the scattered and internal field coefficients of each sphere:

$$c_{l,m}^{(1)} = \tilde{\alpha}_l^{(1)} \sum_\nu \left[a_{\nu,m}^{(2)} A_{m,l,m,\nu}^{(1)} + b_{\nu,m}^{(2)} B_{m,l,m,\nu}^{(1)} \right] - \frac{i n_1}{x_1 G_{\alpha,l}^{(1)}} \eta_{l,m}, \tag{A3}$$

$$d_{l,m}^{(1)} = \tilde{\beta}_l^{(1)} \sum_\nu \left[b_{\nu,m}^{(2)} A_{m,l,m,\nu}^{(1)} + a_{\nu,m}^{(2)} B_{m,l,m,\nu}^{(1)} \right] - \frac{i}{x_1 G_{\beta,l}^{(1)}} \zeta_{l,m}, \tag{A4}$$

$$a_{l,m}^{(2)} = \alpha_l^{(2)} \sum_\nu (-1)^{l+\nu} \left[c_{\nu,m}^{(1)} A_{m,l,m,\nu}^{(1)} - d_{\nu,m}^{(1)} B_{m,l,m,\nu}^{(1)} \right], \tag{A5}$$

$$b_{l,m}^{(2)} = \beta_l^{(2)} \sum_\nu (-1)^{l+\nu} \left[d_{\nu,m}^{(1)} A_{m,l,m,\nu}^{(1)} - c_{\nu,m}^{(1)} B_{m,l,m,\nu}^{(1)} \right], \tag{A6}$$

$$a_{l,m}^{(1)} = \frac{i}{x_1} \frac{c_{l,m}^{(1)}}{\tilde{N}_{\alpha,l}^{(1)}} - \frac{\lambda_l}{\tilde{N}_{\alpha,l}^{(1)}} \eta_{l,m}, \tag{A7}$$

$$b_{l,m}^{(1)} = \frac{i}{n_1 x_1} \frac{d_{l,m}^{(1)}}{\tilde{N}_{\beta,l}^{(1)}} - \frac{\Lambda_l}{\tilde{N}_{\beta,l}^{(1)}} \zeta_{l,m}, \tag{A8}$$

$$c_{l,m}^{(2)} = \frac{i n_2}{n_1 x_2} \frac{1}{N_{\alpha,l}^{(2)}} a_{l,m}^{(2)}, \tag{A9}$$

$$d_{l,m}^{(2)} = \frac{i}{n_1 x_2} \frac{1}{N_{\beta,l}^{(2)}} b_{l,m}^{(2)}, \tag{A10}$$

where we introduce standard (α_l and β_l) and modified ($\tilde{\alpha}_l$ and $\tilde{\beta}_l$) Mie parameters,

$$\tilde{\alpha}_l^{(1)} = -\frac{\tilde{N}_{\alpha,l}^{(1)}}{G_{\alpha,l}^{(1)}}, \quad \tilde{\beta}_l^{(1)} = -\frac{\tilde{N}_{\beta,l}^{(1)}}{G_{\beta,l}^{(1)}}, \qquad \alpha_l^{(2)} = -\frac{N_{\alpha,l}^{(2)}}{G_{\alpha,l}^{(2)}}, \quad \beta_l^{(2)} = -\frac{N_{\beta,l}^{(2)}}{G_{\beta,l}^{(2)}}, \tag{A11}$$

with numerators and denominators defined as

$$\tilde{N}_{\alpha,l}^{(1)} = h_l(n_0 x_1)[n_1 x_1 h_l(n_1 x_1)]' - (n_1/n_0)^2 h_l(n_1 x_1)[n_0 x_1 h_l(n_0 x_1)]', \tag{A12}$$

$$\tilde{N}_{\beta,l}^{(1)} = h_l(n_0 x_1)[n_1 x_1 h_l(n_1 x_1)]' - h_l(n_1 x_1)[n_0 x_1 h_l(n_0 x_1)]', \tag{A13}$$

$$N_{\alpha,l}^{(2)} = j_l(n_1 x_2)[n_2 x_2 j_l(n_2 x_2)]' - (n_2/n_1)^2 j_l(n_2 x_2)[n_1 x_2 j_l(n_1 x_2)]', \tag{A14}$$

$$N_{\beta,l}^{(2)} = j_l(n_1 x_2)[n_2 x_2 j_l(n_2 x_2)]' - j_l(n_2 x_2)[n_1 x_2 j_l(n_1 x_2)]', \tag{A15}$$

$$G_{\alpha,l}^{(i)} = h_l(n x_i)[n_i x_i j_l(n_i x_i)]' - (n_i/n)^2 j_l(n_i x_i)[n x_i h_l(n x_i)]', \tag{A16}$$

$$G_{\beta,l}^{(i)} = h_l(n x_i)[n_i x_i j_l(n_i x_i)]' - j_l(n_i x_i)[n x_i h_l(n x_i)]'. \tag{A17}$$

Additional quantities λ_l and Λ_l in Eqs. (A7) and (A8) are defined as

$$\lambda_l = j_l(n_0 x_1)[n_1 x_1 h_l(n_1 x_1)]' - (n_1/n_0)^2 h_l(n_1 x_1)[n_0 x_1 j_l(n_0 x_1)]', \tag{A18}$$

$$\Lambda_l = j_l(n_0 x_1)[n_1 x_1 h_l(n_1 x_1)]' - h_l(n_1 x_1)[n_0 x_1 j_l(n_0 x_1)]'. \tag{A19}$$

In all these expressions, $[yj_l(y)]' = \frac{d}{d\rho}[\rho j_l(\rho)]|_{\rho=y}$, $x_i = k_0 R_i$, and n_i and n are the vacuum refractive indices of the ith sphere and its surrounding medium, respectively. Note that for sphere 2, the surrounding medium is the first sphere. Functions $A^{(1)}_{m,\nu,m,l}(k,\mathbf{d})$ and $B^{(1)}_{m,\nu,m,l}(k,\mathbf{d})$ are the vector translation coefficients with distance dependence given by spherical Bessel functions [8], where $k = n_1 k_0$ and translation vector $\mathbf{d} = (d,0,0)$. The modified Mie parameters $\tilde{\alpha}^{(1)}_l$ and $\tilde{\beta}^{(1)}_l$ arise in this problem because, unlike the case of the external defect, the field in the interior of the resonator has a radiating component due the presence of the inner sphere. These functions have the same denominators as their respective counterparts $\alpha^{(1)}_l$ and $\beta^{(1)}_l$ and therefore have resonances at the standard Mie poles $x^{(0)}_{s,l} - i\gamma^{(0)}_{s,l}$.

APPENDIX B: TRANSLATION COEFFICIENTS

In this article we follow the conventions for the VSH and the addition theorem employed in [8]. The VSH obey the normalization:

$$\int_0^{2\pi} d\phi \int_0^{\pi} d\theta \sin\theta \mathbf{M}^{(j)}_{l,m} \cdot \mathbf{M}^{(j)*}_{l',m'} = \left[z^{(j)}_l(kr)\right]^2 \delta_{l,l'}\delta_{m,m'}, \tag{B1}$$

$$\int_0^{2\pi} d\phi \int_0^{\pi} d\theta \sin\theta \mathbf{N}^{(j)}_{l,m} \cdot \mathbf{N}^{(j)*}_{l',m'} = \left(\left[\frac{z^{(j)}_l(kr)}{kr} \right]^2 + \left\{ \frac{\left[kr z^{(j)}_l(kr)\right]'}{kr} \right\}^2 \right) \delta_{l,l'}\delta_{m,m'}, \tag{B2}$$

where $[yz_l(y)]' = \frac{d}{dy}[yz_l(y)]$. Consequently, the translation coefficients are defined by

$$\begin{aligned} A^{(j)}_{m',l',m,l}(kd,\theta_t,\phi_t) = {} & \frac{\gamma_{ml}}{\gamma_{m'l'}}(-1)^m \sum_{p=|l-l'|}^{p=|l+l'|} a(m,l;-m',l';p) a(l,l',p) z^{(j)}_p(kd) \\ & \times P^{m-m'}_p(\cos\theta_t) \exp[i(m-m')\phi_t], \end{aligned} \tag{B3}$$

$$\begin{aligned} B^{(j)}_{m',l',m,l}(kd,\theta_t,\phi_t) = {} & \frac{\gamma_{ml}}{\gamma_{m'l'}}(-1)^{m+1} \sum_{p=|l-l'|}^{p=|l+l'|} a(m,l;-m',l';p,p-1) b(l,l',p) z^{(j)}_p(kd) \\ & \times P^{m-m'}_p(\cos\theta_t) \exp[i(m-m')\phi_t], \end{aligned} \tag{B4}$$

where

$$a(m,l;m',l';p) = (-1)^{m+m'}(2p+1)\sqrt{\frac{(l+m)!(l'+m')!(p-m-m')!}{(l-m)!(l'-m')!(p+m+m')!}} \begin{pmatrix} l & l' & p \\ m & m' & -(m+m') \end{pmatrix} \begin{pmatrix} l & l' & p \\ 0 & 0 & 0 \end{pmatrix}, \tag{B5}$$

$$a(m,l;m',l';p,q) = (-1)^{m+m'}(2p+1)\sqrt{\frac{(l+m)!(l'+m')!(p-m-m')!}{(l-m)!(l'-m')!(p+m+m')!}} \begin{pmatrix} l & l' & p \\ m & m' & -(m+m') \end{pmatrix} \begin{pmatrix} l & l' & q \\ 0 & 0 & 0 \end{pmatrix}, \tag{B6}$$

$$a(l,l',p) = \frac{i^{l'-l+p}(2l'+1)}{2l'(l'+1)}[l(l+1) + l'(l'+1) - p(p+1)], \tag{B7}$$

$$b(l,l',p) = -\frac{i^{l'-l+p}(2l'+1)}{2l'(l'+1)}\sqrt{(l+l'+1+p)(l+l'+1-p)(p+l-l')(p-l+l')}, \tag{B8}$$

$$\gamma_{ml} = \sqrt{\frac{(2l+1)(l-m)!}{4\pi l(l+1)(l+m)!}}, \tag{B9}$$

and $P^{m-m'}_p(\cos\theta_t)$ are the associated Legendre polynomials. The symbols

$$\begin{pmatrix} l & l' & p \\ m & m' & -(m+m') \end{pmatrix} \tag{B10}$$

are the Wigner $3j$ symbols [8].

[1] J. W. Strutt (B. Rayleigh) *Scientific Papers* (Cambridge University Press, Cambridge, 1899), Vol. 1.
[2] K. J. Vahala, Nature (London) **424**, 839 (2003).
[3] M. L. Gorodetsky, A. D. Pryamikov, and V. S. Ilchenko, J. Opt. Soc. Am. B **17**, 1051 (2000).
[4] D. S. Weiss, V. Sandoghdar, J. Hare, V. Lefèvre-Seguin, J.-M. Raimond, and S. Haroche, Opt. Lett. **20**, 1835 (1995).
[5] B. E. Little, J. P. Juha-Pekka Laine, and S. T. Chu, Opt. Lett. **22**, 4 (1997).
[6] T. J. Kippenberg, S. M. Spillane, and K. J. Vahala, Opt. Lett. **27**, 1669 (2002).
[7] M. Borselli, T. Johnson, and O. Painter, Opt. Express **13**, 1515 (2005).
[8] M. I. Mishchenko, L. D. Travis, and A. A. Lacis, *Scattering, Absorption and Emission of Light by Small Particles* (Cambridge University Press, Cambridge, UK, 2002).
[9] A. Mazzei, S. Götzinger, L. de S. Menezes, G. Zumofen, O. Benson, and V. Sandoghdar, Phys. Rev. Lett. **99**, 173603 (2007).
[10] T. M. Benson, S. V. Boriskina, P. Sewell, A. Vukovic, S. C. Greedy, and A. I. Nosich, *Micro-optical Resonators for Microlasers and Integrated Optoelectronics* (Springer, Netherlands, 2006), Vol. 216 of *Frontiers in Planar Lightwave Circuit Technology, NATO Science Series*, p. 39.
[11] G. Mie, Ann. Phys. **330**, 377 (1908).
[12] A. T. Rosenberger (private communication).
[13] K. A. Fuller, Appl. Opt. **30**, 4716 (1991).
[14] H. Miyazaki and Y. Jimba, Phys. Rev. B **62**, 7976 (2000).
[15] L. I. Deych, C. Schmidt, A. Chipouline, T. Pertsch, and A. Tünnermann, Phys. Rev. A **77**, 051801 (2008).
[16] J. Bruning and Y. Lo, IEEE Trans. Antennas Propag. **19**, 378 (1971).
[17] J. Bruning and Y. Lo, IEEE Trans. Antennas Propag. **19**, 391 (1971).
[18] K. Fuller and G. Kattawar, Opt. Lett. **13**, 90 (1988).
[19] K. Fuller and G. Kattawar, Opt. Lett. **13**, 1063 (1988).
[20] Y. Xu, Appl. Opt. **34**, 4573 (1995).
[21] J. Fikioris and N. Uzunoglu, J. Opt. Soc. Am. **69**, 1359 (1979).
[22] B. Yan, X. Han, and K. Ren, J. Opt. A **11**, 015705 (2009).
[23] K. Fuller, J. Opt. Soc. Am. A **12**, 893 (1995).
[24] L. Deych and J. Rubin, Phys. Rev. A **80**, 061805(R) (2009).
[25] O. R. Cruzan, Q. Appl. Math. **20**, 33 (1962).
[26] K. T. Kim, *Progress in Electromagnetics Research* (EMW Publishing, Cambridge, MA, 2004), Vol. 48.
[27] M. Abramowitz and I. Stegun, *Handbook of Mathematical Functions with Formulas, Graphs and Mathematical Tables* (National Bureau of Standards, Washington, DC, 1972).
[28] B. Knoll and F. Keilmann, Opt. Commun. **182**, 321 (2000).
[29] Y. Hara, T. Mukaiyama, K. Takeda, and M. Kuwata-Gonokami, Phys. Rev. Lett. **94**, 203905 (2005).
[30] C. P. Dettmann, G. V. Morozov, M. Sieber, and H. Waalkens, Europhys. Lett. **82**, 34002 (2008).
[31] J. G. Zhu, S. K. Ozdemir, Y. F. Xiao, L. Li, L. N. He, D. R. Chen, and L. Yang, Nat. Photonics **4**, 46 (2010).